AIAA JOURNAL
Vol. 33, No. 1, January 1995

Numerical Study of Sound Generation due to a Spinning Vortex Pair

Duck Joo Lee* and Sam Ok Koo†
Korea Advanced Institute of Science and Technology, Yusung, Taejon 305-701, Korea

A numerical approach for the calculation of an acoustic field is applied to the case of a spinning vortex pair to investigate the sound generation by quadrupole sources in unsteady vortical flows. Based on the unsteady hydrodynamic information from the known incompressible flowfield, the perturbed compressible acoustic terms derived from the Euler equations are calculated. Nonreflecting boundary conditions are developed to obtain highly stable solutions. Calculated results are compared with analytical solutions obtained by the method of matched asymptotic expansions. The possibility of predicting the effect of convective mean flow is also tested. It is concluded that the sound generated by the quadrupole sources of unsteady vortical flows without a sound-generating body or surface can be calculated by using the source terms of hydrodynamic flow fluctuations.

Nomenclature

$\boldsymbol{A}, \boldsymbol{B}$ = Jacobian matrices
a_0 = ambient speed of sound
b = vortex position in complex domain
$\boldsymbol{C}, \boldsymbol{C}'$ = source terms in acoustic equations
$\boldsymbol{E}, \boldsymbol{F}$ = flux vectors in the x and y directions
f = frequency
$H_2^{(2)}(kr)$ = second kind Hankel function of order 2
i = imaginary number
k = wave number
$\boldsymbol{l}_i$ = left eigenvectors of $\boldsymbol{A}$
$\boldsymbol{M}$ = diagonal matrix of $\boldsymbol{B}$
M_r = rotating Mach number
P = hydrodynamic pressure
$\bar{P}$ = time-mean of hydrodynamic pressure
p' = acoustic pressure
$\boldsymbol{P}, \boldsymbol{Q}, \boldsymbol{R}$ = Jacobian matrices in Eq. (11)
$Re\{\}$ = real part of a complex number or function
r_c = core radius of a vortex model
r_0 = radius of rotation of vortex pair
$\boldsymbol{S}, \boldsymbol{T}$ = eigenvector matrices of $\boldsymbol{A}$ and $\boldsymbol{B}$
T = period of rotation
t = time
$\boldsymbol{U}$ = vector of primitive variables
$\tilde{\boldsymbol{U}}$ = vector of conservative variables
U, V = hydrodynamic velocity components in the x and y directions
u', v' = acoustic velocity components in the x and y directions
V_θ = tangential velocity
x, y = Cartesian coordinates
z = a position in the complex domain
Γ = intensity of circulation
γ = ratio of specific heats
Δt = time step
θ = angular argument of a position in complex domain
$\boldsymbol{\Lambda}$ = diagonal matrix of $\boldsymbol{A}$
λ_i = eigenvalue of $\boldsymbol{A}$
ρ_0 = ambient density
ρ_1 = hydrodynamic density correction
ρ' = acoustic density
σ_t = weighting factor in time step
Φ = complex potential function
Φ_0 = steady part of complex potential function
Φ_1 = fundamental term in complex potential function
ω = angular velocity

I. Introduction

STUDIES on sound generation by unsteady flowfields in the presence or in the absence of a body are important to the understanding and solving of many noise problems of practical interest; for example, blade-vortex interaction, edge tones, and jet noise. The motion of vorticity is considered to be directly related to the source of sound generated by vortical flows, and vortex-induced flows have been studied both theoretically[1–5] and numerically[6–10] by many researchers. In accordance with the developments in computational fluid dynamics (CFD), computational aeroacoustics (CAA) provides a useful tool in analyzing the mechanism of aeroacoustic sound generation and propagation. There are several approaches in CAA to calculate sound. Hardin and Lamkin[11] and Hardin and Pope[12] calculated the far-field sound by using the Green function based on an unsteady hydrodynamic flowfield solution obtained by a standard CFD technique. Colonius et al.[9] Mitchell et al.,[10] Tam and Webb,[13] and Lele[14] have obtained results by direct simulation of Navier–Stokes equations. Direct simulation of Navier–Stokes equations is the most desirable method, but it requires a higher order numerical scheme. Huh et al.[15] and Watson and Myers[16] solved the perturbed acoustic equations derived from the Euler equations to calculate propagation, scattering, or diffraction of incoming waves. However, the perturbed Euler equations can not predict the sound generated by inherent unsteadiness of the flow because of the homogeneity of the equations.

In a recent paper, Hardin and Pope[17] proposed a new computational aeroacoustics technique, where they split the Euler equations into the hydrodynamic terms and the perturbed acoustic terms. The novelty of their approach is found in the introduction of a new variable named hydrodynamic density fluctuations, which is the basic difference in the formulation of governing equations from others.[15,16] They applied the technique to the problems of a pulsating sphere and an oscillating sphere, which were acting as a monopole or a dipole source with sound-generating body surfaces. More recently, Hardin and Pope[18] applied their method to describe a cavity flow.

In the present paper, we numerically studied the sound generation by purely quadrupole sources. The acoustic field induced by a spinning vortex pair is calculated because it has analytic solutions and represents the basic acoustic field generated by turbulent shear flows, jet flows, edge tones, etc. The goals of this study are to verify the applicability of the CAA technique to calculate the

Presented at the AIAA 15th Aeroacoustics Conference, Long Beach, CA, Oct. 25–27, 1993; received Jan. 27, 1994; revision received July 18, 1994; accepted for publication July 19, 1994. Copyright © 1994 by the American Institute of Aeronautics and Astronautics, Inc. All rights reserved.

*Associate Professor, Department of Aerospace Engineering. Member AIAA.

†Graduate Student, Department of Aerospace Engineering; also Senior Researcher at Korea Aerospace Research Institute.

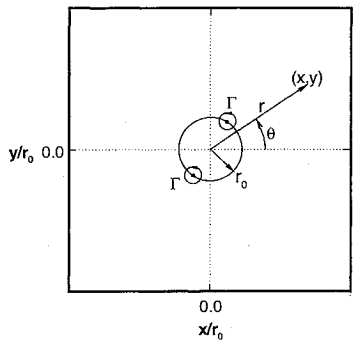

Fig. 1 Schematic diagram of flow configuration.

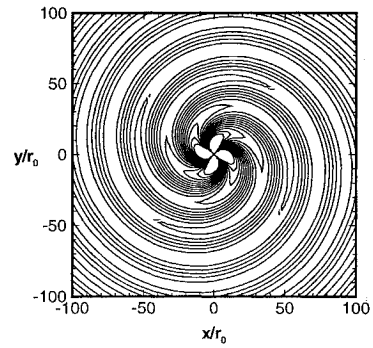

Fig. 2 Analytical acoustic pressure contour for $\Gamma/a_0 r_0 = 1.0, M_r = 0.0796$.

sound field generated by a purely unsteady vortical flow, to study associated numerical problems such as boundary conditions and vortex models, and to investigate the basic physics of compressible sound generation due to the incompressible flow fluctuations. The hydrodynamic terms are obtained from the analytical solutions of the spinning vortex pair in this numerical study.

II. Flow Description

The flowfield induced by a spinning vortex pair can be assumed as inviscid and incompressible. The two point-vortices, separated by a distance of $2r_0$, with circulation intensity of Γ, as illustrated in Fig. 1, result in corotation of the vortices along a circular path with radius r_0, period $T = 8\pi^2 r_0^2/\Gamma$, rotating speed $\omega = \Gamma/4\pi r_0^2$, and rotating Mach number $M_r = \Gamma/4\pi r_0 a_0$. The rotating noncircular streamlines are directly associated with the hydrodynamic field of the rotating quadrupole.[1]

III. Theoretical Analysis

Theoretical analysis by the method of matched asymptotic expansions (MAE) for spinning vortices was first performed by Müller and Obermeier[2] and is also discussed in Obermeier.[19] In the method of MAE, the solution of the equations for incompressible motion in the flow domain and a homogeneous compressible wave equation in the acoustic field are matched in an intermediate domain in such a way as to give an asymptotically valid solution.

The incompressible, inviscid flow, which can also be considered as the inner solution of the acoustic field, induced by a pair of vortices can be expressed by a complex potential function $\Phi(z, t)$

$$\Phi(z,t) = \frac{\Gamma}{2\pi i}\ln(z-b) + \frac{\Gamma}{2\pi i}\ln(z+b) = \frac{\Gamma}{2\pi i}\ln z^2\left(1-\frac{b^2}{z^2}\right) \tag{1}$$

where $z = re^{i\theta}$, and $b = r_0 e^{i\omega t}$. For $|z/b| \gg 1$, Eq. (1) can be approximated by

$$\Phi(z,t) \approx \frac{\Gamma}{\pi i}\ln z - \frac{\Gamma}{2\pi i}\left(\frac{b}{z}\right)^2 = \Phi_0 + \Phi_1 \tag{2}$$

The first term on the right-hand side of Eq. (2) represents a steady vortical flow, whereas the second term represents the fluctuation with the fundamental frequency due to the vortex motion.

The outer acoustic field, which is the perturbed compressible flowfield, is governed by the homogeneous wave equation

$$\nabla^2\Phi - \frac{1}{a_0^2}\frac{\partial^2\Phi}{\partial t^2} = 0 \tag{3}$$

With appropriate matching conditions and harmonic assumptions, a matched asymptotic expansion solution of the complex potential representing the leading quadrupole term is obtained as

$$\Phi(z,t) = \frac{\Gamma k^2 r_0^2}{8} H_2^{(2)}(kr) e^{-i2(\theta-\omega t)} \tag{4}$$

where $k = 2\omega/a_0$.

The far-field solution for the acoustic pressure can be obtained from Eq. (4) as

$$p'(z,t) = -\rho_0 \frac{\partial}{\partial t}\Phi(z,t) \tag{5}$$

The amplitude of the pressure fluctuations [Eq. (5)] is the real part of the following equation:

$$p'(r) = \frac{\rho_0 \Gamma k^2 r_0^2 \omega}{4} H_2^{(2)}(kr) = \frac{\rho_0 \Gamma^4}{64\pi^3 r_0^4 a_0^2} H_2^{(2)}(kr) \tag{6}$$

A typical contour plot of Eq. (6) is a double-spiral pattern of a rotating quadrupole as shown in Fig. 2.

IV. Computational Analysis

Governing Equations

According to the technique proposed by Hardin and Pope,[17] the governing equations derived from the Euler equations for two-dimensional acoustic fields induced by unsteady, inviscid flow can be expressed in a nondimensional form as

$$\frac{\partial \tilde{\boldsymbol{U}}}{\partial t} + \frac{\partial \boldsymbol{E}}{\partial x} + \frac{\partial \boldsymbol{F}}{\partial y} = -\boldsymbol{C}' \tag{7}$$

where

$$\tilde{\boldsymbol{U}} = \begin{bmatrix} \rho' \\ (1+\rho_1+\rho')u' + \rho' U \\ (1+\rho_1+\rho')v' + \rho' V \end{bmatrix}$$

$$\boldsymbol{E} = \begin{bmatrix} (1+\rho_1+\rho')u' + \rho' U \\ (1+\rho_1+\rho')(2Uu' + u'^2) + U^2\rho' + p' \\ (1+\rho_1+\rho')(Vu' + Uv' + u'v') + UV\rho' \end{bmatrix}$$

$$\boldsymbol{F} = \begin{bmatrix} (1+\rho_1+\rho')v' + \rho' V \\ (1+\rho_1+\rho')(Vu' + Uv' + u'v') + UV\rho' \\ (1+\rho_1+\rho')(2Vv' + v'^2) + V^2\rho' + p' \end{bmatrix}$$

$$\boldsymbol{C}' = \begin{bmatrix} \dfrac{\partial \rho_1}{\partial t} + \dfrac{\partial(\rho_1 U)}{\partial x} + \dfrac{\partial(\rho_1 V)}{\partial y} \\ \dfrac{\partial}{\partial t}(\rho_1 U) + \dfrac{\partial}{\partial x}(\rho_1 U^2) + \dfrac{\partial}{\partial y}(\rho_1 UV) \\ \dfrac{\partial}{\partial t}(\rho_1 V) + \dfrac{\partial}{\partial x}(\rho_1 UV) + \dfrac{\partial}{\partial y}(\rho_1 V^2) \end{bmatrix}$$

and with

$$p' = \frac{1}{\gamma}(1+\rho_1+\rho')^\gamma - P$$

using the isentropic assumption.

The density, velocity, and pressure variables in Eq. (7) are nondimensionalized by ρ_0, a_0, and $\rho_0 a_0^2$, respectively. The length and time variables in Eq. (7) are nondimensionalized by r_0 and r_0/a_0, respectively. In Eq. (7) ρ', u', v', and p' are the perturbed compressible acoustic density, velocities, and pressure, respectively; and U, V, and P are the incompressible hydrodynamic solutions of time-dependent velocity components, and pressure, respectively. The variable ρ_1 is the key parameter, which relates the incompressible hydrodynamic flowfield as the sound source to the compressible acoustic field. The parameter ρ_1 is defined by the isentropic relation as

$$\rho_1 = \frac{1}{a_0^2}(P - \bar{P}) \tag{8}$$

where

$$\bar{P} = \lim_{T\to\infty} \frac{1}{T}\int_0^T P\,\mathrm{d}t$$

The hydrodynamic velocity is obtained by differentiating Eq. (1) with respect to z, and the hydrodynamic pressure P is obtained by the unsteady Bernoulli's equation as

$$U - iV = \frac{\partial \Phi(z,t)}{\partial z} \tag{9}$$

$$P = P_0 - \rho_0 \frac{\partial}{\partial t}\{\mathrm{Re}(\Phi(z,t))\} - \tfrac{1}{2}\rho(U^2 + V^2) \tag{10}$$

Boundary Conditions

Nonreflecting boundary conditions based on Thompson's[20] technique are used in solving Eq. (7), because they are straightforward and easy to apply. However, as indicated by Watson and Myers,[21] Thompson's boundary conditions have the limitation of not reproducing the outgoing acoustic solutions except for planar waves. The acoustic field of interest can be considered as quasiplanar along the far boundary of the domain. To compensate for the limitations, additional physical boundary conditions are considered here and applied to the problem. It will be described after the original boundary conditions of Thompson.[20]

First, to apply the boundary conditions, Eq. (7) is linearized and recast in the following form:

$$\boldsymbol{P}\frac{\partial \boldsymbol{U}}{\partial t} + \boldsymbol{Q}\frac{\partial \boldsymbol{U}}{\partial x} + \boldsymbol{R}\frac{\partial \boldsymbol{U}}{\partial y} = -\boldsymbol{C}' \tag{11}$$

where

$$\boldsymbol{U} = [\rho', u', v']^T$$

$$\boldsymbol{P} = \frac{\partial \tilde{\boldsymbol{U}}}{\partial \boldsymbol{U}}, \qquad \boldsymbol{Q} = \frac{\partial \boldsymbol{E}}{\partial \boldsymbol{U}}, \qquad \boldsymbol{R} = \frac{\partial \boldsymbol{F}}{\partial \boldsymbol{U}}$$

or

$$\frac{\partial \boldsymbol{U}}{\partial t} + \boldsymbol{A}\frac{\partial \boldsymbol{U}}{\partial x} + \boldsymbol{B}\frac{\partial \boldsymbol{U}}{\partial y} = -\boldsymbol{C} \tag{12}$$

where

$$\boldsymbol{A} = \boldsymbol{P}^{-1}\boldsymbol{Q}, \qquad \boldsymbol{B} = \boldsymbol{P}^{-1}\boldsymbol{R}, \qquad \boldsymbol{C} = \boldsymbol{P}^{-1}\boldsymbol{C}'$$

Matrices $\boldsymbol{A}$ and $\boldsymbol{B}$ are diagonalizable by the similarity transformations

$$\boldsymbol{S}\boldsymbol{A}\boldsymbol{S}^{-1} = \boldsymbol{\Lambda}, \qquad \boldsymbol{T}\boldsymbol{B}\boldsymbol{T}^{-1} = \boldsymbol{M} \tag{13}$$

where the diagonal elements of $\boldsymbol{\Lambda}$ and $\boldsymbol{M}$ are the eigenvalues of $\boldsymbol{A}$ and $\boldsymbol{B}$ and can easily be obtained as

$$\boldsymbol{\Lambda} = \mathrm{diag}(U - 1, 1, U + 1)$$

and

$$\boldsymbol{M} = \mathrm{diag}(V - 1, 1, V + 1) \tag{14}$$

where U and V are the hydrodynamic velocity components.

Along the x boundaries, Eq. (7) is rewritten as

$$\frac{\partial \tilde{\boldsymbol{U}}}{\partial t} + \frac{\partial \boldsymbol{F}}{\partial y} + \boldsymbol{C}' + \boldsymbol{P}\left(\boldsymbol{S}^{-1}\boldsymbol{\Lambda}\boldsymbol{S}\frac{\partial \boldsymbol{U}}{\partial x}\right) = 0 \tag{15}$$

Abbreviating the quantity in parentheses as $-\partial \boldsymbol{U}/\partial t_x$, a characteristic equation is derived as

$$\boldsymbol{S}\frac{\partial \boldsymbol{U}}{\partial t_x} + \boldsymbol{\Lambda}\boldsymbol{S}\frac{\partial \boldsymbol{U}}{\partial x} = 0 \tag{16}$$

or

$$\boldsymbol{l}_i\frac{\partial \boldsymbol{U}}{\partial t_x} + \lambda_i \boldsymbol{l}_i\frac{\partial \boldsymbol{U}}{\partial x} = 0 \tag{17}$$

where $\boldsymbol{l}_i$ are left eigenvectors of $\boldsymbol{A}$ and λ_i are eigenvalues of $\boldsymbol{A}$. Thompson's nonreflecting boundary condition is expressed in the general form by rewriting Eq. (17) as

$$\boldsymbol{l}_i\frac{\partial \boldsymbol{U}}{\partial t_x} + \mathcal{L}_i = 0 \tag{18}$$

where

$$\mathcal{L}_i = \begin{cases} \lambda_i \boldsymbol{l}_i \dfrac{\partial \boldsymbol{U}}{\partial x} & \text{for outgoing waves} \\ 0 & \text{for incoming waves} \end{cases}$$

The same procedure is performed along the y boundaries.

As mentioned previously, the physical boundary conditions are also considered. The basic concept is that the acoustic wave radiating through the far boundary is nearly cylindrical and is thought to be locally planar with nondimensional acoustic impedance of 1. This physical condition with an isentropic assumption gives the relations

$$p' = u'_{\mathrm{radial}} = \rho' \tag{19}$$

In the modified boundary conditions only ρ' (the first component of $\boldsymbol{U}$) is calculated by Eq. (18), and the remaining two components are evaluated by the relations (19). The differences between the original Thompson's boundary conditions and modified ones are discussed in Sec. V.

Numerical Method

MacCormack's predictor-corrector scheme has gained wide use and acceptance for solving time-dependent problems in fluid dynamics[15,17] and is used in the present study to integrate both the interior and the boundary points of Eq. (7).

Predictor step

$$\tilde{\boldsymbol{U}}_{i,j} = \boldsymbol{U}^n_{i,j} - \frac{\Delta t}{\Delta x}\left(\boldsymbol{E}^n_{i+1,j} - \boldsymbol{E}^n_{i,j}\right) - \frac{\Delta t}{\Delta y}\left(\boldsymbol{F}^n_{i,j+1} - \boldsymbol{F}^n_{i,j}\right) - \Delta t \cdot \boldsymbol{C}'_{i,j} \tag{20}$$

Corrector step

$$\boldsymbol{U}^{n+1}_{i,j} = \frac{1}{2}\left[\boldsymbol{U}^n_{i,j} + \tilde{\boldsymbol{U}}_{i,j} - \frac{\Delta t}{\Delta x}(\tilde{\boldsymbol{E}}_{i,j} - \tilde{\boldsymbol{E}}_{i-1,j}) - \frac{\Delta t}{\Delta y}(\tilde{\boldsymbol{F}}_{i,j} - \tilde{\boldsymbol{F}}_{i,j-1}) - \Delta t \cdot \tilde{\boldsymbol{C}}'_{i,j}\right] \tag{21}$$

Equations (18) and (19) are applied for the boundary conditions.

The time step for Eqs. (20) and (21) to meet the CFL criterion is determined according to Refs. 15 and 22 as

$$\Delta t = \sigma_t / \Delta t_c \tag{22}$$

where

$$\Delta t_c = \left[\frac{|U|}{\Delta x} + \frac{|V|}{\Delta y} + a_0\sqrt{\frac{1}{(\Delta x)^2} + \frac{1}{(\Delta y)^2}}\right]$$

and σ_t is a positive constant less than 1. In the present calculations, $\sigma_t = 0.9$ is used.

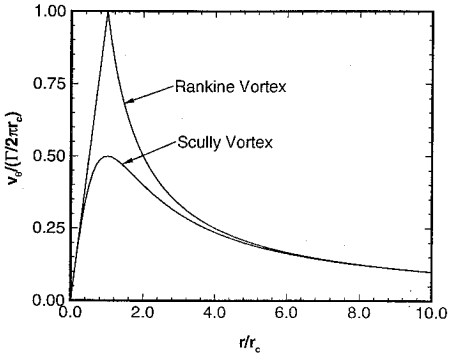

Fig. 3 Vortex velocity profiles around core.

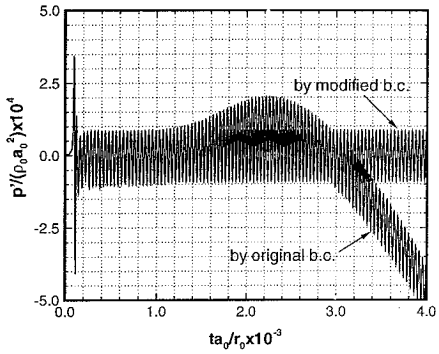

Fig. 4 Time history of acoustic pressure at far field for Γ/a_0r_0 = 1.0, M_r = 0.0796.

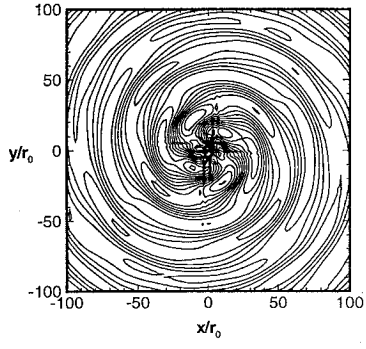

Fig. 5 Calculated acoustic pressure contour with Rankine vortex model for Γ/a_0r_0 = 1.0, M_r = 0.0796.

Vortex-Core Models

In the numerical analysis for the acoustic field due to spinning vortices, a vortex-core model is required to avoid the singularity at the center of the vortex. Two different vortex-core models are investigated in the present study: the Rankine and the Scully[23] models.[24] The two models are described as follows.

Rankine model

$$V_\theta = \begin{cases} \dfrac{\Gamma r}{2\pi r_c^2} & (0 \le r \le r_c) \\ \dfrac{\Gamma}{2\pi r} & (r > r_c) \end{cases} \tag{23}$$

Scully model

$$V_\theta = \frac{\Gamma r}{2\pi\left(r_c^2 + r^2\right)} \tag{24}$$

where V_θ is the tangential velocity, r a radial distance from the vortex center, and r_c is the core radius.

The tangential velocity distributions of the two models are compared in Fig. 3. The Scully model has smoother velocity distribution, whereas the Rankine model has a discontinuity in the slope of its velocity and vorticity.

V. Results and Discussion

Numerical studies are carried out for various circulation intensities Γ and spinning radii r_0 of the vortex pair over a square domain of dimension $L \times L$ with an equidistance rectangular grid system. All of the calculations begin with the initial fluctuation quantities set to zero. The vortices are assumed to start spinning abruptly at time $t = 0$. Analytical solutions to the hydrodynamic flowfield are evaluated at each time step over the computational domain and are used as the source terms in Eq. (7).

Effect of Boundary Conditions

The acoustic signal propagated to a given far-field point of $x/r_0 = 100$, $y/r_0 = 0$ is plotted in Fig. 4. No noticeable signal is observed until the nondimensional time $ta_0/r_0 \cong 100$, and steady harmonic wave propagation is achieved after $ta_0/r_0 \cong 400$ for the case shown in Fig. 4. The intensity of circulation is $\Gamma/a_0r_0 = 1.0$, the rotating Mach number is $M_r = 0.0796$, the period is $Ta_0/r_0 = 79.05$, and the quadrupole frequency is $fr_0/a_0 = 0.0253$. The result using Thompson's boundary conditions is identical to the one using modified boundary conditions until nondimensional time $ta_0/r_0 \cong 1000$, which corresponds to about 12 periods of rotation. As time marches, the solution using the original Thompson's boundary conditions begins to deteriorate because of the reflected noise. However, the solution using the present modified boundary conditions remains stable.

Acoustic Fields

As noted previously in Sec. III, a typical acoustic pressure contour obtained by the method of matched asymptotic expansion is shown in Fig. 2 for the case of the vortex pair of circulation $\Gamma/a_0r_0 = 1.0$ and rotating Mach number $M_r = 0.0796$. Contour lines are plotted for a range of $-0.0003 \le p'/\rho_0a_0^2 \le 0.0003$ with a step increment of 0.0004. The application of the modified boundary conditions provided highly stable solutions as illustrated in Fig. 4, but the contour lines still have some irregularities over the domain as shown in Fig. 5. The reason for the irregularities is thought to be the discontinuity of vorticity in the Rankine vortex-core model. The Rankine model has a discontinuity in vorticity at $r = r_c$ (core radius), whereas the Scully model has a smoothly varying vorticity distribution around the vortex core. The discontinuity of vorticity in space also generates the discontinuity in time for the source terms in the near field. Figures 6a–6c show the results with the Scully vortex-core model for the same case shown in Figs. 2 and 5. A contour plot for the acoustic pressure is shown in Fig. 6a. A comparison of the acoustic pressure profiles with the theoretical result is shown in Fig. 6b along a radial line from the center to the lower-right corner of the domain. Figure 6c shows a three-dimensional graphical view of the acoustic pressure field, where the z axis represents the acoustic pressure exaggerated 200 times. It is thought that the Scully vortex model shows more realistic features of the flow, and it is adopted in all of the other results.

A case for a lower rotational frequency is shown in Figs. 7a and 7b, where the intensity of circulation Γ/a_0r_0 is 0.6, the frequency is 0.0152, and the rotating Mach number is 0.0477. In Fig. 7a, the acoustic pressure profile at an instant along a radial line from the center to the lower-right corner of the domain is compared with the result given by MAE, showing good agreement. Figure 7b is the three-dimensional graphical view of the acoustic pressure field, where the z axis represents 10^3 times the acoustic pressure. Figures 8a and 8b show a case for a stronger sound source, i.e., higher rotating Mach number, where the intensity of circulation Γ/a_0r_0 is 1.6, the frequency fr_0/a_0 is 0.0405, and $M_r = 0.1273$. The analytical and numerical acoustic pressure profile is compared in Fig. 8a, and the three-dimensional graphical view of the acoustic field is shown in Fig. 8b. The scaling factor of the z axis in Fig. 8b is 50.

It is noted that the intensity of the sound source is directly related to the rotating Mach number. As theoretically obtained by Müller and Obermeier,[2] the intensity of the sound from spinning vortices

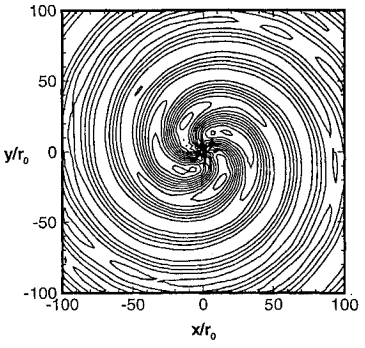

Fig. 6a Acoustic pressure contour for $\Gamma/a_0r_0 = 1.0, M_r = 0.0796$ with Scully vortex model.

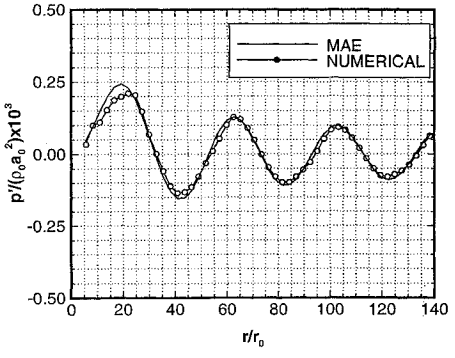

Fig. 6b Comparison of acoustic pressure distribution for $\Gamma/a_0r_0 = 1.0$, $M_r = 0.0796$ with Scully vortex model.

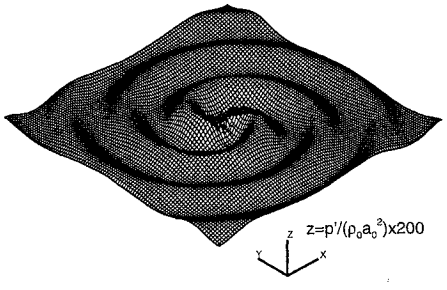

Fig. 6c Three-dimensional graphical view of acoustic field for $\Gamma/a_0r_0 = 1.0, M_r = 0.0796$ with Scully vortex model.

is proportional to M_r in the compact limit. According to Yates,[4] the compact limit is asymptotically valid for the rotating Mach number M_r less than 0.1. Figures 6b and 7a, which represent the cases within the compact limit, show good agreements in phase and amplitude compared with the MAE solutions. But, Fig. 8a for $M_r = 0.1273$ shows some discrepancy. However, such figures of acoustic pressure profiles do not provide sufficient information to discuss the compactness.

Spectral Analysis

The time history of the acoustic pressure signal observed at a given far-boundary point is sampled after the solution reaches a stable oscillation, and its Fourier transform is obtained by a fast Fourier transform (FFT) algorithm. The power spectral density (PSD) of the acoustic signal is obtained as the squared magnitude of its Fourier transform.

As noted in Refs. 7 and 10, the octupole and higher order terms begin to dominate as the rotating Mach number (M_r) exceeds 0.1. The acoustical compactness is described in terms of the ratio between wavelength (λ) and rotating radius λ/r_0. The case of $M_r = 0.1$ corresponds to $\lambda/r_0 = 31.4$. The acoustic time signals observed at a given point ($x/r_0 = 100$, $y/r_0 = 0$) are analyzed in the spectral domain, and the results are shown in Fig. 9. The PSD reveals not only the fundamental frequency but also the higher harmonics. The PSD for the MAE solution is also obtained by the same procedure

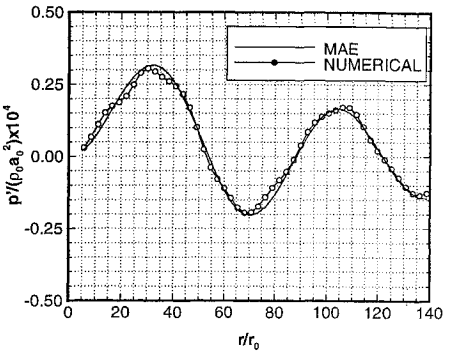

Fig. 7a Comparison of acoustic pressure distribution for $\Gamma/a_0r_0 = 0.6, M_r = 0.0477$.

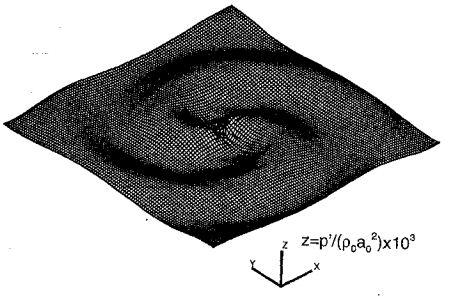

Fig. 7b Three-dimensional graphical view of acoustic field for $\Gamma/a_0r_0 = 0.6, M_r = 0.0477$.

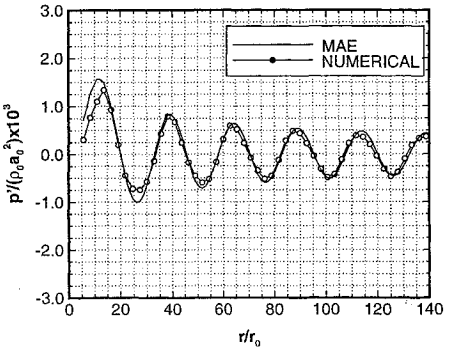

Fig. 8a Comparison of acoustic pressure distribution for $\Gamma/a_0r_0 = 1.6$, $M_r = 0.1273$.

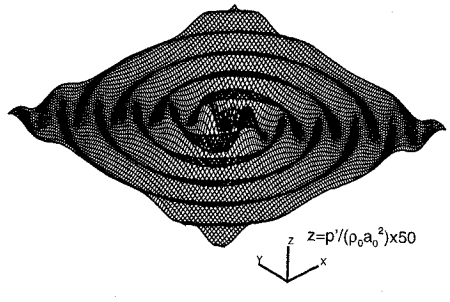

Fig. 8b Three-dimensional graphical view of acoustic field for $\Gamma/a_0r_0 = 1.6, M_r = 0.1273$.

as used for the numerical solution. It is noted that the PSD for the MAE solution has only one peak (fundamental frequency) because the octupole and higher harmonic terms are ignored in the analysis.

Figure 9a corresponds to $\Gamma/a_0r_0 = 0.6$, $M_r = 0.0477$, and the fundamental frequency of 0.0152; and Fig. 9b corresponds to $\Gamma/a_0r_0 = 1.0$, $M_r = 0.0796$, and the fundamental frequency of 0.0253. Comparison of the results obtained by the numerical and MAE methods shows good agreement, as expected in the compact source limit. Octupole and higher multipoles are also detected in the numerical results. Based on Yates' analysis, the difference in sound power between a quadrupole and an octupole is about 47 dB and 38 dB for

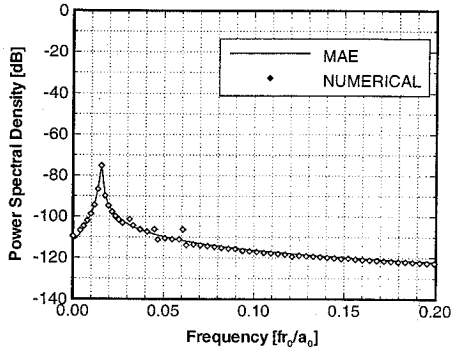

a)

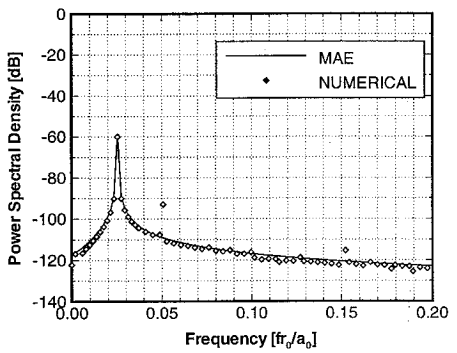

b)

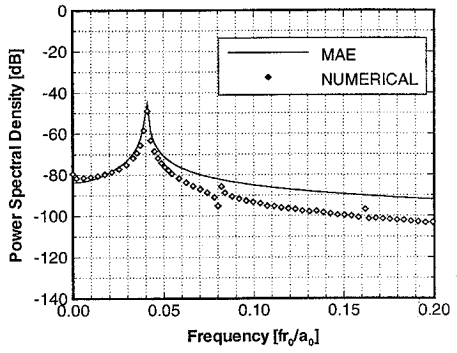

c)

Fig. 9 Power spectral density of acoustic pressure for a) $\Gamma/a_0r_0 = 0.6$, $M_r = 0.0477$, b) $\Gamma/a_0r_0 = 1.0$, $M_r = 0.0796$, and c) $\Gamma/a_0r_0 = 1.6$, $M_r = 0.1273$.

the same conditions of Figs. 9a and 9b respectively. The difference in the PSD of the present numerical study is about 26 dB and 33 dB for the same cases.

Figure 9c corresponds to $\Gamma/a_0r_0 = 1.6$, $M_r = 0.1273$, and the fundamental frequency of 0.0405. Comparison of the PSDs shows that the MAE solution overpredicts the sound power for this case, where an M_r of 0.1273 is above the compact limit. This trend agrees with Yates' analysis. Figure 9c also shows the octupole and higher multipoles. The difference in the PSD between the quadrupole and the octupole frequency is about 36 dB, which also shows a comparable difference to the theoretical difference of about 30 dB in sound power based on Yates' analysis. The 30-dB difference in power corresponds to a 31.6 times difference in the acoustic pressure, which is negligible in sound power. However, to resolve the octupole and the higher multipole terms more accurately, a higher order scheme should be used, at the cost of more computational effort.

Effect of Convective Flow

A more general acoustic field of spinning vortices in a convective flow has also been calculated. A uniform flow of Mach number 0.3 is linearly superposed on the spinning-vortices flowfield of

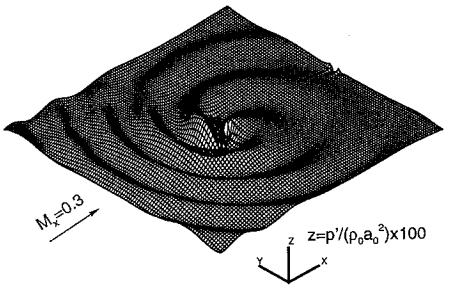

Fig. 10a Three-dimensional graphical view for $\Gamma/a_0r_0 = 1.0$, $M_r = 0.0796$, $M_x = 0.3$.

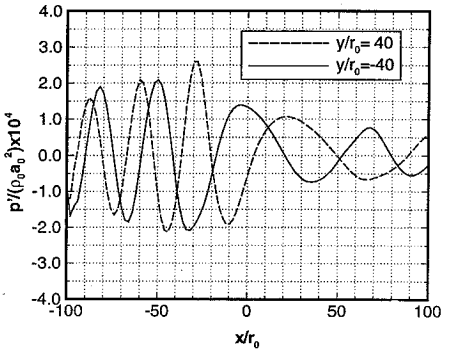

Fig. 10b Acoustic pressure distributions for $\Gamma/a_0r_0 = 1.0$, $M_r = 0.0796$, $M_x = 0.3$.

$\Gamma/a_0r_0 = 1.0$, and $M_r = 0.0796$. Figure 10a is a three-dimensional graphical view of the simulated acoustic pressure field, where the z axis represents acoustic pressure fluctuations exaggerated 100 times. Pressure fluctuations along $y/r_0 = -40$ and $y/r_0 = 40$ lines are plotted in Fig. 10b. Increase and decrease in the amplitude and wave numbers (decrease in wavelength) are observed at upstream and downstream locations, respectively. The Doppler effects in the amplitude and wave numbers of convective flow are well captured.

VI. Conclusions

A computational aeroacoustic technique, which splits Euler equations into the hydrodynamic terms and the perturbed acoustic terms, is applied to the case of a spinning vortex pair. It is found that the sound generated by the quadrupole source of unsteady vortical flows in the absence of a sound-generating body surface (monopole or dipole source) can be calculated by using the source terms due to the hydrodynamic pressure fluctuations. Appropriate modeling of the vortex core is necessary to avoid oscillations of the solutions to the problems considered. The Scully vortex-core model shows better results than the Rankine model. Nonreflecting boundary conditions are developed to obtain highly stable solutions. Spectral analysis is shown to be a good tool to analyze the signal in the acoustic field, and the extension of the study to nonuniform convective flow has been shown to be straightforward.

References

[1]Powell, A., "Theory of Vortex Sound," *Journal of the Acoustical Society of America*, Vol. 36, No. 1, 1964, pp. 177–195.

[2]Müller, E.-A., and Obermeier, F., "The Spinning Vortices as a Source of Sound," AGARD CP-22, 1967, pp. 22.1–22.8.

[3]Möhring, W., "On Vortex Sound at Low Mach Number," *Journal of Fluid Mechanics*, Vol. 85, P. 4, 1978, pp. 685–691.

[4]Yates, J. E., "Application of the Bernoulli Enthalpy Concept to the Study of Vortex Noise and Jet Impingement Noise," NASA CR 2987, 1978.

[5]Kambe, T., "Acoustic Emissions by Vortex Motions," *Journal of Fluid Mechanics*, Vol. 173, 1986, pp. 643–666.

[6]Lee, D. J., and Chae, K. S.,"Calculation of Vortex-Airfoil-Interaction by using a Vortex-In-Cell Method," *Proceedings of the 27th Aircraft Symposium*, 1989, pp. 574–577.

[7]Lee, D. J., and Smith, C. A., "Effect of Vortex Core Distortion on Blade-Vortex Interaction," *AIAA Journal*, Vol. 29, No. 9, 1991, pp. 1355–1362.

[8]Park, J. H., and Lee, D. J., "Numerical Simulation of Vortex-Wedge

Interaction, " *AIAA Journal*, Vol. 32, No. 6, 1994, pp. 1126–1134.

[9]Colonius, T., Lele, S. K., and Moin, P., "Scattering of Sound Waves by a Compressible Vortex," AIAA Paper 91-0494, 1991.

[10]Mitchell, B. E., Lele, S. K., and Moin, P., "Direct Computation of the Sound From a Compressible Co-Rotating Vortex Pair," AIAA Paper 92-0374, 1992.

[11]Hardin, J. C., and Lamkin, S. L., "Aeroacoustic Computation of Cylinder Wake Flow," *AIAA Journal*, Vol. 22, No. 1, 1984, pp. 51–57.

[12]Hardin, J. C., and Pope, D. S., "Sound Generated by a Stenosis in a Pipe," AIAA Paper 90-3919, 1990.

[13]Tam, C. K. W., and Webb, J. C., "Dispersion-Relation-Preserving Schemes for Computational Aeroacoustics," DGLR/AIAA 92-02-033, May 1992.

[14]Lele, S. K., "Direct Numerical Simulation of Compressible Free Shear Flows," AIAA Paper 89-0374, Jan. 1989.

[15]Huh, K. S., Agrawal, R. K., and Widnall, S. E., "Numerical Simulation of Acoustic Diffraction of Two-Dimensional Rigid Bodies in Arbitrary Flows," AIAA Paper 90-3920, 1990.

[16]Watson, W. R., and Myers, M. K., "A Two-Step Method for Evolving Acoustic Systems to a Steady-State," AIAA Paper 90-3946, 1990.

[17]Hardin, J. C., and Pope, D. S., "A New Technique for Aerodynamic Noise Calculation," DGLR/AIAA 92-02-076, 1992.

[18]Hardin, J. C., and Pope, D.S., "Sound Generation by Flow over a Two-Dimensional Cavity," AIAA Paper 93-4327, 1993.

[19]Obermeier, F., "The Application of Singular Perturbations Methods to Aerodynamic Sound Generation," *Singular Perturbations and Boundary Layer Theory*, edited by Brauner, Gray and Mathieu, Springer-Verlag, Berlin, 1977, pp. 401–421.

[20]Thompson, K. W., "Time Dependent Boundary Conditions for Hyperbolic Systems, " *Journal of Computational Physics*, Vol. 68, 1987, pp. 1–24.

[21]Watson, W. R., and Myers, M. K., "Inflow-Outflow Boundary Conditions for Two-Dimensional Acoustic Waves in Channels with Flow," *AIAA Journal*, Vol. 29, No. 9, 1991, pp. 1383–1389.

[22]Anderson, D. A., Tannehill, J. C., and Pletcher, R. H., *Computational Fluid Mechanics and Heat Transfer*, McGraw-Hill, New York, 1984.

[23]Scully, M. P., "Computation of Helicopter Rotor Wake Geometry and Its Influence on Rotor Harmonic Airloads," Massachusetts Inst. of Technology, Pub. ARSL TR 178-1, Cambridge, MA, March 1975.

[24]Stremel, P. M., "A Method for Modelling Finite Core Vortices in Wake Flow Calculations," AIAA Paper 84-0417, Jan. 1984.